On the numerical evaluation of the prolate spheroidal wave functions of order zero

James Bremer

Department of Mathematics, University of Toronto

Abstract

We describe a method for the numerical evaluation of the angular prolate spheroidal wave functions of the first kind of order zero. It is based on the observation that underlies the WKB method, namely that many second order differential equations admit solutions whose logarithms can be represented much more efficiently than the solutions themselves. However, rather than exploiting this fact to construct asymptotic expansions of the prolate spheroidal wave functions, our algorithm operates by numerically solving the Riccati equation satisfied by their logarithms. Its running time grows much more slowly with bandlimit and characteristic exponent than standard algorithms. We illustrate this and other properties of our algorithm with numerical experiments.

Keywords: fast algorithms, special functions, spheroidal wave functions, ordinary differential equations

1. Introduction

Many families of special functions are defined by second order linear ordinary differential equations whose coefficients depend on one or more parameters. The cost to represent solutions of such equations using standard methods, such as polynomial and trigonometric expansions, typically grows quite quickly with magnitudes of the parameters. It is well known, though, that in many cases there exist solutions whose logarithms can be represented at a cost which is bounded independent of the parameters, or at least grows extremely slowly with them.

This observation is the basis of many approaches to the asymptotic approximation of the solutions of second order linear ordinary differential equations. The WKB method, for instance, can be used to construct asymptotic expansions of the solutions of equations of the form

$$y''(t) + \lambda^2 q(t) y(t) = 0 \tag{1}$$

with q a strictly positive smooth function. In this case, there exist a solution y of (1) and a sequence of functions $r_0, r_1, \ldots$ which depend on q and its derivatives, but not λ, such that

$$y(t) = \exp\left(i \sum_{n=0}^{N} \lambda^{1-n} \, r_n(t) \right) \left(1 + \mathcal{O}\left(\lambda^{-N}\right)\right) \quad \text{as} \quad \lambda \to \infty \tag{2}$$

(see, for instance, Section 7.2 of [17]). The solution y is oscillatory and the cost of representing it with standard methods grows linearly with λ. By contrast, the functions r_n can be represented at

Email address: `bremer@math.toronto.edu` (James Bremer)

a cost which depends only on the complexity of q, and not on λ. This means that for sufficiently large values of λ, it is much more efficient to represent y via (2) than to construct a polynomial expansion of y itself.

Asymptotic methods allow for the evaluation of many special functions in time independent of the parameters they depend on, but are only accurate for sufficiently large values of those parameters. They are often coupled with methods which are accurate at all values of the parameters, but whose running times grow with the parameters, to obtain efficient algorithms for the numerical evaluation of a family of special functions. This is the approach used in [3], for instance, to evaluate the Legendre polynomials in time independent of their degree. Further examples can be found in [4, 18, 9] and their references. Unfortunately, in many cases existing asymptotic expansions are either not amenable to numerical evaluation or only achieve high-accuracy at extremely large values of the parameters, making such an approach infeasible.

The prolate spheroidal wave functions of order zero and bandlimit $\gamma > 0$ are an example of a family of special functions for which such an approach is not viable. They are the solutions of the second order linear ordinary differential equation

$$(1 - z^2)y''(z) - 2zy'(z) + (\chi - \gamma^2 z^2)y(z) = 0, \tag{3}$$

which we call the reduced spheroidal wave equation (reduced because it is obtained from the more familiar spheroidal wave equation by deleting one parameter). The solutions of most interest are those which satisfy the boundary conditions

$$\lim_{z \to \pm 1} y'(z)\sqrt{1 - z^2} = 0. \tag{4}$$

Together (3) and (4) constitute a singular self-adjoint Sturm-Liouville problem. Consequently, there exists a sequence

$$\chi_0(\gamma) < \chi_1(\gamma) < \chi_2(\gamma) < \cdots \tag{5}$$

of values of the parameter χ for which solutions of (3) satisfying (4) exist. For each $\chi_n(\gamma)$, there is a corresponding one-dimensional space of solutions of (3), and we use $Ps_n(z;\gamma)$ to denote the particular element of that subspace which agrees with the Legendre function $P_n(z)$ at the point $z = 0$. The parameter n usually called the characteristic exponent — this term comes from the standard mechanism used to define $Ps_\nu(z;\gamma)$ for noninteger ν — and $Ps_n(z;\gamma)$ is known as the angular prolate spheroidal wave function of the first kind of bandlimit γ, order 0 and characteristic exponent n.

Although uniform asymptotic expansions of the $Ps_n(z;\gamma)$ are available [5], they only achieve high accuracy for extremely large values of γ and involve a complicated change of variables, thus making them difficult to exploit in numerical computations. This leaves algorithms whose running times increase fairly rapidly with γ and n as the only viable mechanisms for the numerical evaluation of $Ps_n(z;\gamma)$. The standard approach is the Osipov-Xiao-Rokhlin algorithm [19, 20]. It proceeds by solving an eigenproblem for a symmetric tridiagonal matrix in order to construct a Legendre expansion representing the desired prolate function. The dependence of the running time of this algorithm on the parameters γ and n is not fully understood, but the numerical experiments of [22] suggest that it behaves as $\mathcal{O}\left(n + \sqrt{\gamma n}\right)$ for large values of the parameters.

We describe an algorithm for evaluating $Ps_n(z;\gamma)$ whose running time grows much more slowly with γ and n. It operates by solving the Riccati equation satisfied by the logarithms of the solutions of the reduced spheroidal wave equation numerically. Most solutions of that equation are no easier to represent than the prolate spheroidal wave function themselves. However, standard

results (such as those appearing in Section 7.2 of [17]) imply that there is a "WKB solution" of the reduced spheroidal wave equation whose logarithm can be asymptotically approximated by a series of relatively simple functions. It is straightforward to identify this solution from well-known formulas, and it is the logarithm of this solution we construct by solving the Riccati equation. Based on the numerical experiments discussed in this article, we believe that the cost of representing it via polynomial expansions grows sublogarithmically with γ and is bounded independent of n for fixed γ. The running time of our algorithm displays the same dependence on γ and n.

We also state several conjectures about the monotonicity properties of the modulus of this WKB solution. These conjectures are relevant because the logarithm of any solution of a second order differential equation is related to the modulus of the solution through a simple formula. Our conjectures assert that the monotonicity properties of the reduced spheroidal wave equation are similar to those of Legendre's differential equation, which it generalizes.

There are two significant limitations of the algorithm described in this paper. First, it requires knowledge of Sturm-Liouville eigenvalue $\chi_n(\gamma)$ in order to calculate $Ps_n(z;\gamma)$. Second, while the running time of our algorithm grows much more slower with γ and n than does the Osipov-Rokhlin-Xiao algorithm, the later is more efficient until fairly large values of γ and n. The author remedies these problems in a separate article, which describes a method for computing the value of $\chi_n(\gamma)$ in time independent the parameters as well as an approach to accelerating the algorithm of this paper which makes it faster than the Osipov-Xiao-Rokhlin algorithm except at extremely small values of the parameters. A comparison of the running times of the unaccelerated and accelerated versions of the algorithm of this paper and the Xiao-Osipov-Rokhlin method can be found in Section 6 of this paper.

The remainder of this article is structured as follows. Section 2 briefly discuss the Riccati equation satisfied by the logarithms of solutions of second order linear ordinary differential equations. In Section 3, we discuss the prolate spheroidal wave functions of order zero. In Section 4, the monotonicity properties of Legendre's differential equation are described and we make several conjectures regarding the monotonicity properties of the reduced spheroidal wave equation. Section 5 details our numerical algorithm for the evaluation of the prolate spheroidal wave functions of order zero. In Section 6, we describe the results of numerical experiments which were conducted to demonstrate the properties of our algorithm. We close with a few brief remarks in Section 7.

2. Riccati's equation and its variants

A straightforward calculation shows that if $y(x) = \exp(r(x))$ solves the second order differential equation

$$y''(x) + q(x)y(x) = 0, \tag{6}$$

then r satisfies the Riccati equation

$$r''(x) + (r'(x))^2 + q(x) = 0. \tag{7}$$

We note that under extremely mild regularity conditions on its coefficients, any second order linear ordinary differential equation can be put into the form (6) through a simple transformation (see, for instance, Section 5.6 of [12]).

By inserting the expression $r(x) = \pm i\psi(x) + \beta(x)$ into (7), it can be shown that if ψ and β satisfy

the system of equations

$$\begin{cases} \beta''(x) + (\beta'(x))^2 - (\psi'(x))^2 + q(x) = 0 \\ \psi''(x) + 2\psi'(x)\beta'(x) = 0, \end{cases} \tag{8}$$

then r solves (7). The second equation in (8) admits the formal solution

$$\beta(x) = -\frac{1}{2}\log(\psi'(x)), \tag{9}$$

which when inserted into the first equation in (8) results in

$$q(x) - (\psi'(x))^2 + \frac{3}{4}\left(\frac{\psi''(x)}{\psi'(x)}\right)^2 - \frac{1}{2}\frac{\psi'''(x)}{\psi'(x)} = 0. \tag{10}$$

Equation (10) is known as Kummer's equation after E. E. Kummer who studied it in [14]. Clearly, if ψ does not vanish in an open interval and it satisfies Kummer's equation there, then

$$r_1(x) = i\psi(x) - \frac{1}{2}\log(\psi'(x)) \quad \text{and} \quad r_2(x) = -i\psi(x) - \frac{1}{2}\log(\psi'(x)) \tag{11}$$

are solutions of Riccati's equation on that interval. It follows that

$$u(x) = \frac{\sin(\psi(x))}{\sqrt{\psi'(x)}} \quad \text{and} \quad v(x) = \frac{\cos(\psi(x))}{\sqrt{\psi'(x)}} \tag{12}$$

constitute a basis in the space of solutions of (6). In this event, we refer to ψ as a phase function for (6). We note that the realization of the square root used in (12) is immaterial. For obvious reasons,

$$m(x) = (u(x))^2 + (v(x))^2 = \frac{1}{\psi'(x)} \tag{13}$$

is known as the modulus function associated with ψ. It can be readily verified that m satisfies the differential equation

$$m'''(x) + 4q(x)m'(x) + 2q'(x)m(x) = 0, \tag{14}$$

which we refer to as Appell's equation after P. E. Appell, who discussed it in [1].

Given any pair u, v of solutions of (6) whose Wronskian is $w \neq 0$ and such that such that the modulus function (13) is nonzero in an open interval I, it can be shown by a straightforward calculation that

$$\psi'(x) = \frac{w}{(u(x))^2 + (v(x))^2} \tag{15}$$

satisfies (10) on that interval. It follows that any antiderivative of ψ' is a phase function for (6) on I. Requiring that (12) holds determines ψ up to an integral multiple of 2π, but further restrictions are required to determine it uniquely. We note that on any set where u and v are real-valued, the modulus function (13) is nonzero since independent solutions of a second order differential equation cannot simultaneously vanish.

Because of the close relationship between the functions ψ, m and r, we regard them all as representations of the logarithm of a solution of (6). Moreover, we view Equations (7), (10) and (14) as essentially interchangeable mechanisms for computing the logarithm of a solution of (6).

3. The prolate spheroidal wave functions of order zero

In this section, we briefly discuss certain facts regarding the prolate spheroidal wave functions of order zero which will be used in the algorithm of this paper.

3.1. The angular prolate spheroidal wave functions of the first kind

In addition to being the solutions of a singular self-adjoint Sturm-Liouville, the angular prolate spheroidal wave functions of bandlimit $\gamma > 0$, order zero and integer characteristic exponents

$$Ps_0(z;\gamma),\ Ps_1(z;\gamma),\ Ps_2(z;\gamma),\ \ldots \tag{16}$$

are the eigenfunctions of the restricted Fourier operator

$$\mathscr{F}_\gamma\left[f\right](z) = \int_{-1}^{1} \exp\left(i\gamma z t\right) f(t)\ dt. \tag{17}$$

As such, they provide an efficient mechanism for representing elements of the image of $\mathscr{F}_\gamma$, which is the set of functions with bandlimit γ. The dual nature of the functions (16) was widely publicized in an article [23] published in the 1960s, but it was known much earlier (see, for instance, Section 3.8 of [16] and the references cited there).

It is shown in [15] that the magnitudes of the first $2/\pi\gamma$ or so eigenvalues of $\mathscr{F}_\gamma$ are close to $\sqrt{2\pi/\gamma}$, the magnitudes of the next $\mathcal{O}\left(\log(\gamma)\right)$ eigenvalues decay extremely rapidly, and the remaining eigenvalues are all close to zero. It follows that only the first $2/\pi\gamma + \mathcal{O}\left(\log(\gamma)\right)$ of the functions (16) are needed to represent elements of the image of $\mathscr{F}_\gamma$, which is the space of functions with bandlimit γ, with extremely high relative accuracy. In other words, for the purposes of numerical computation, the dimension of the space of functions with bandlimit γ is $2/\pi\gamma + \mathcal{O}\left(\log(\gamma)\right)$.

The reduced spheroidal wave equation (3) has a regular singular point at $z = 1$ and zero is a double root of the corresponding indicial equation. Consequently, there is a one-dimensional subspace of solutions which are regular at $z = 1$ and all other solutions have logarithmic singularities there (see, for instance, Chapter 5 of [12]). Because it is an eigenfunction of the restricted Fourier operator, $Ps_n(z;\gamma)$ is entire and so the subspace of solutions which are regular at $z = 1$ comprises its multiples. Every other solution has a logarithmic singularity at 1.

Since $Ps_n(z;\gamma)$ is an eigenfunction of (17), there exists a constant $A_n(\gamma)$ such that

$$Ps_n(z;\gamma) = A_n(\gamma)\frac{\sin\left(\gamma z\right)}{\gamma z}\left(1 + \mathcal{O}\left(\frac{1}{z}\right)\right) \quad \text{as} \quad z \to \infty. \tag{18}$$

It is a consequence of this and the fact that $Ps_n(z;\gamma)$ is regular at 1 that $Ps_n(z;\gamma)$ is an element of $L^2(1,\infty)$.

3.2. The radial prolate spheroidal wave function of the third kind of order zero

Another solution of the reduced spheroidal wave equation, which is known as the radial prolate spheroidal wave function of the third kind of order zero, is defined via the formula

$$S_n^{(3)}(z;\gamma) = \frac{1}{Ps_n(1,\gamma)}\int_1^\infty \exp(i\gamma z t) Ps_n(t;\gamma)\ dt. \tag{19}$$

Since $Ps_n(z;\gamma)$ is in $L^2(1,\infty)$, the integral is absolutely convergent for all $\mathrm{Im}(z) > 0$ and $S_n^{(3)}(z;\gamma)$ is usually taken to be function obtained by analytically continuing it to the cut plane $\mathbb{C}\backslash\{-\infty, 1\}$. However, for our purposes, it is more convenient to take its domain to be $\{z : \mathrm{Im}(z) \geqslant 0\}\backslash\{-1, 1\}$. The asymptotic behaviour of $S^{(3)}(z;\gamma)$ is obvious from Formula (19):

$$S_n^{(3)}(z;\gamma) = \frac{\exp\left(i\gamma z\right)}{\gamma z}\left(1 + \mathcal{O}\left(\frac{1}{z}\right)\right) \quad \text{as} \quad z \to \infty. \tag{20}$$

3.3. Two variants of the reduced spheroidal wave equation

We shall make use of two variants of the reduced spheroidal wave equation of the form (6). The first of these is

$$y_1''(x) + \left(\frac{\exp(x) - \frac{1}{4}}{(1 - 2\exp(x))^2} + \chi \, \frac{2\exp(x) - 1}{(1 - 2\exp(x))^2} - \gamma^2 \exp(-2x) \right) y_1(x) = 0, \quad 0 < x < \infty, \tag{21}$$

which is satisfied by any function of the form $y_1(t) = y\,(1 - \exp(-x))\sqrt{2 - \exp(-x)}$ with y a solution of (3). We refer to (21) as the exponential form of the reduced spheroidal wave equation. Our motivation for introducing this exponential change of variables will be explained in Section 5.

Similarly, if y is a solution of (3) on the upper half of the imaginary axis, then $y_2(t) = y(it)\sqrt{1 + t^2}$ satisfies

$$y_2''(t) - \left(\frac{1}{(1 + t^2)^2} + \frac{\chi + \gamma^2 t^2}{1 + t^2} \right) y_2(t) = 0, \quad 0 < t < \infty. \tag{22}$$

3.4. The phase and modulus functions associated with $S_n^{(3)}(z;\gamma)$

Since the coefficient in (21) is real-valued, the real and imaginary parts of

$$S_n^{(3)}(1 - \exp(-x);\gamma)\sqrt{2 - \exp(-x)} \tag{23}$$

are separately solutions. Accordingly,

$$M_n(1 - \exp(-x);\gamma)(2 - \exp(-x)), \tag{24}$$

where

$$M_n(z;\gamma) = \left| S_n^{(3)}(z;\gamma) \right|^2, \tag{25}$$

is a modulus function for (21). Since the Wronskian of any pair of solutions of (21) is necessarily constant, it follows from (20) that the Wronskian of the pair of solutions consisting of the real and imaginary parts of $S_n^{(3)}(z;\gamma)$ is γ and we define $\Psi S_n(x;\gamma)$ on the interval $[0,\infty)$ via

$$\Psi S_n(x;\gamma) = \int_\infty^x \frac{\gamma}{M_n(1 - \exp(-u);\gamma)(2 - \exp(-u))} \, du. \tag{26}$$

It follows from the discussion in Section 2 that $\Psi S_n(x;\gamma)$ is a phase function for the exponential form of the reduced spheroidal wave equation. In particular,

$$\frac{\sin\left(\Psi S_n(x;\gamma)\right)}{\sqrt{\frac{d\Psi S_n}{dx}(x;\gamma)}} \quad \text{and} \quad \frac{\cos\left(\Psi S_n(x;\gamma)\right)}{\sqrt{\frac{d\Psi S_n}{dx}(x;\gamma)}} \tag{27}$$

form a basis in the space of solutions of Equation (21). Moreover, (26) ensures that

$$\lim_{x\to\infty} \Psi S_n(x;\gamma) = 0. \tag{28}$$

Since $Ps_n(1 - \exp(-x);\gamma)\sqrt{2 - \exp(-x)}$, is a solution of the exponential form of the reduced spheroidal wave equation, there exist constants $C_n(\gamma)$ and $D_n(\gamma)$ such that

$$Ps_n(1 - \exp(-x);\gamma)\sqrt{2 - \exp(-x)} = C_n(\gamma)\frac{\sin\left(\Psi S_n(x;\gamma)\right)}{\sqrt{\frac{d\Psi S_n}{dx}(x;\gamma)}} + D_n(\gamma)\frac{\cos\left(\Psi S_n(x;\gamma)\right)}{\sqrt{\frac{d\Psi S_n}{dx}(x;\gamma)}}. \tag{29}$$

In fact, we claim that condition (28) ensures $D_n(\gamma) = 0$ in (29); that is, our choice of the constant of integration for $\Psi S_n(x;\gamma)$ guarantees that $Ps_n(1 - \exp(-x);\gamma)\sqrt{2 - \exp(-x)}$ is a multiple of

$$\frac{\sin\left(\Psi S_n(x;\gamma)\right)}{\sqrt{\frac{d\Psi S_n}{dx}(x;\gamma)}}.$$

To see this, we first observe that (29) holds if and only if if

$$\begin{aligned} Ps_n(1-\exp(-x);\gamma) = & \frac{C_n(\gamma)}{\sqrt{\gamma}}\sqrt{M_n(1-\exp(-x);\gamma)}\sin\left(\Psi S_n(x;\gamma)\right) \\ & + \frac{D_n(\gamma)}{\sqrt{\gamma}}\sqrt{M_n(1-\exp(-x);\gamma)}\cos\left(\Psi S_n(x;\gamma)\right). \end{aligned} \tag{30}$$

Next, we note that since every solution of the reduced spheroidal wave equation which is not a multiple of $Ps_n(z;\gamma)$ has a logarithmic singularity at 1,

$$\lim_{x\to\infty} M_n(1-\exp(-x);\gamma) = \lim_{z\to 1^-} M_n(z;\gamma) = \infty. \tag{31}$$

Equations (28) and (31) imply that

$$\lim_{x\to\infty}\sqrt{M_n(1-\exp(-x);\gamma)}\cos\left(\Psi S_n(x;\gamma)\right) = \infty, \tag{32}$$

whereas $Ps_n(x;\gamma)$ is nonsingular at $x=1$. It follows that the constant $D_n(\gamma)$ in (30) must be 0.

4. Montonicity properties of the reduced spheroidal wave equation

Many second order differential equations admit solutions whose logarithms are easier to represent, either numerically or symbollically, then the solutions themselves. Because of the close relationship between the logarithms of solutions of second order linear ordinary differential equations and their modulus functions, this is often demonstrated by establishing the existence of modulus functions satisfying certain monotonicity properties.

From (20), it is clear that $S_n^{(3)}(z;\gamma)$ is a "WKB solution" of the reduced spheroidal wave equation in that, at least for large values of z, its logarithm can be approximated by a polynomial expansion at cost which is independent of γ and n. In fact, plotting its modulus function for various values of n and γ suggests that the modulus function associated with $S_n^{(3)}(z;\gamma)$ satisfies rather strong monotonicity properties (see Figure 1 for representative plots).

In this section, we first discuss the monotonicity properties of a certain modulus function for Legendre's differential equation. Then, we conjecture that the modulus function corresponding to $S_\nu(z;\gamma)$ behaves in a similar fashion.

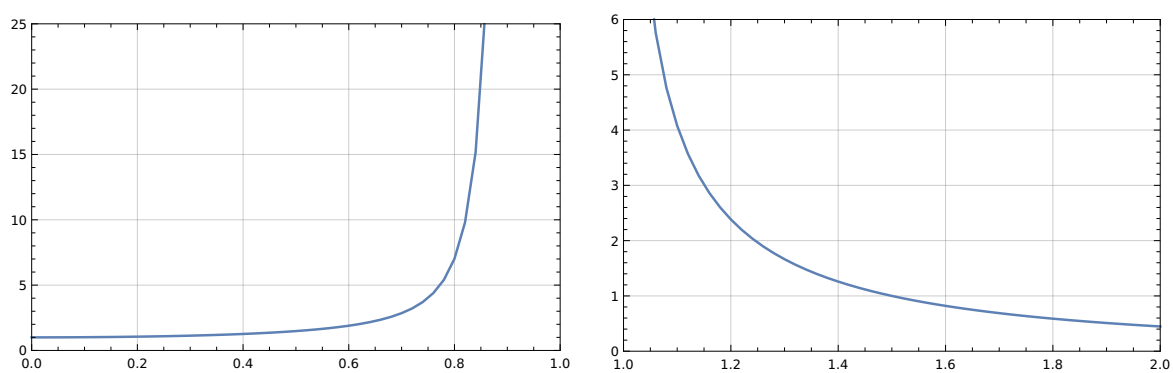

Figure 1: On the left is a plot of $\left|S_n^{(3)}(x;\gamma)\right|^2$ over the interval $(0,1)$ when $\gamma=20$ and $n=10$. On the right, is a plot of the same function over the interval $(1,2)$.

4.1. Completely, absolutely and multiply monotone functions

A function f defined on an open interval I is k-times monotone there provided $(-1)^j f^{(j)}(z) \geqslant 0$ for all nonnegative integers $j \leqslant k$ and all $z \in I$. It is completely monotone if $(-1)^k f^{(k)}(z) \geqslant 0$ for

all nonnegative integers k and all $z \in I$. Finally, f is absolutely monotone if $f^{(k)}(z) \geqslant 0$ for all nonnegative k and all $z \in I$. It is well known that f is completely monotone on $(0, \infty)$ if and only if it is the Laplace transform of a nonnegative Borel measure (see, for instance, Chapter 4 of [25] for a proof of this).

4.2. Legendre's differential equation

Legendre's differential equation, which is the special case of (3) when $\gamma = 0$, is a classical example of a differential equation admitting a modulus function which satisfies various monotonicity properties. The Legendre function of the second kind of degree ν is given by

$$Q_\nu(z) = \exp\left(-i\frac{\pi}{2}(\nu+1)\right)\int_0^\infty \exp(izt) j_\nu(t)\, dt, \tag{33}$$

where j_ν denotes the spherical Bessel function of order ν. The integral is absolutely convergent for $\mathrm{Im}(z) > 0$ and $Q_\nu(z)$ is typically defined to be the function obtained by analytically continuing the integral (33) to the cut plane $\mathbb{C}\setminus(-\infty, 1]$. However, we prefer to takes its domain to be the set $\{z : \mathrm{Im}(z) \geqslant 0\}\setminus\{-1, 1\}$.

It can be easily verified that $Q_\nu(x)\sqrt{1-x^2}$ satisfies the differential equation

$$y''(x) + \left(\frac{1}{(1-x^2)^2} + \frac{\chi}{1-x^2}\right) y(x) = 0, \quad -1 < x < 1, \tag{34}$$

where $\chi = \nu(\nu+1)$. Since the coefficient in (34) is real-valued, the real and imaginary parts of this function are separately solutions, and $|Q_\nu(x)|^2 (1-x^2)$ is a modulus function for (34). Because

$$j_\nu(t) \sim \frac{\sin\left(t - \frac{\pi}{2}\nu\right)}{t} \quad \text{as} \quad t \to \infty, \tag{35}$$

the contour in (33) can be shifted from the real axis to the imaginary axis whenever $\mathrm{Re}(z) > 1$. This results in the formula

$$Q_\nu(z) = \exp\left(-i\frac{\pi}{2}(\nu+1)\right)\int_0^\infty \exp(-zt) i_\nu(t)\, dt \tag{36}$$

with i_ν the modified spherical Bessel function of the first kind of order ν. Since i_ν is positive on $(0, \infty)$, (36) implies that $Q_\nu(x)$ is completely monotone on the interval $(1, \infty)$. From this and the formula

$$|Q_\nu(x)|^2 = \int_1^\infty Q_\nu\left(x^2 + (1-x^2)t\right) \frac{dt}{\sqrt{t^2-1}}, \tag{37}$$

which holds for $\nu \geqslant 0$ and can be found in [7], it follows that $|Q_\nu(x)|^2$ is absolutely monotone on the interval $(-1, 1)$ when $\nu \geqslant 0$. Since the square of a completely monotone function is completely monotone, we have the following theorem summarizing the monotonicity properties of $|Q_\nu(x)|^2$:

Theorem 1. *For fixed $\nu \geqslant 0$, $|Q_\nu(x)|^2$ is absolutely monotone on $(0, 1)$ and completely monotone on $(1, \infty)$.*

4.3. The reduced spheroidal wave equation

Many other second order linear ordinary differential equations admit modulus functions which satisfy various monotonicity properties. Relevant formulas for the Jacobi functions, Gegenbauer functions and Hermite functions can be found in [7], and the articles [10] and [11] give conditions under which a second order linear ordinary differential equation admits a completely monotone modulus function.

However, to the author's knowledge, no results concerning the monotonicity properties of the reduced spheroidal wave equation appear in the literature. Since the reduced spheroidal wave

equation (3) generalizes Legendre's differential equation, it is reasonable to suspect that the solution $S_n^{(3)}(z;\gamma)$ behaves similarly to $Q_n(z)$. This is further suggested by the many similaries between Formulas (19) and (33). Accordingly, we make the following conjecture regarding the radial prolate spheroidal wave function of the third kind:

Conjecture 1. *For fixed $\gamma > 0$ and $n \geqslant 0$, $M_n(z;\gamma)$ is absolutely monotone on $(0,1)$ and completely monotone on $(1,\infty)$.*

Since the coefficient in (22) is negative for $u \in (0,\infty)$, the function $S_n^{(3)}(iu;\gamma)$ is nonoscillatory for $0 < u < \infty$. Based on experiments performed using computer algebra systems, we make the following conjecture regarding the behavior of $S_n^{(3)}(z;\gamma)$ on the imaginary axis:

Conjecture 2. *For fixed $\gamma > 0$ and $n \geqslant 0$, $S_n^{(3)}(iu;\gamma)$ is $(2+n)$-times monontone on the interval $(0,\infty)$.*

Remark 1. *In [21], we discuss the standard mechanism for defining $S_\nu^{(3)}(z;\gamma)$ for noninteger values of ν and generalize Conjectures 1 and 2 to that case.*

5. Numerical algorithm

We now describe our algorithm for the numerical evaluation of $Ps_n(z;\gamma)$. In addition to the values of γ and n, it takes as input the Sturm-Liouville eigenvalue $\chi_n(\gamma)$ and a positive integer k. The algorithm operates by constructing a kth order piecewise Chebyshev expansion representing the phase function $\Psi S_n(x;\gamma)$ on an interval of the form $[0,\beta)$. More explicitly, the piecewise Chebyshev expansion comprises a partition

$$0 = x_0 < x_1 < x_2 < \ldots < x_n = \beta \tag{38}$$

of $[0,\beta)$ together with the coefficients $\{a_{ij} : 1 \leqslant i \leqslant n,\ 1 \leqslant j \leqslant k\}$ in the expansion

$$\Psi S_n(x;\gamma) \approx \sum_{i=1}^{n} I_{[x_{i-1},x_i)}(x) \sum_{j=0}^{k} a_{ij}\ T_j\left(\frac{2}{x_i - x_{i-1}}x + \frac{x_{i-1}+x_i}{x_{i-1}-x_i}\right), \tag{39}$$

where T_j denotes the Chebyshev polynomial of degree and $I_{[x_{i-1},x_i)}(x)$ is the characteristic function

$$I_{[x_{i-1},x_i)}(x) = \begin{cases} 1 & \text{if } \ x_{i-1} \leqslant x < x_i \\ 0 & \text{otherwise.} \end{cases} \tag{40}$$

In all of the experiments described in this paper, we took $k = 29$ and $\beta = 10^{120}$. We will shortly explain why such a large value of β is needed.

The phase function is related to $Ps_n(z;\gamma)$ via the formula

$$Ps_n(z;\gamma) = C_n(\gamma)\frac{\sin\left(\Psi S_n(x;\gamma)\right)}{\sqrt{(1+z)\frac{d\Psi S_n}{dx}(x;\gamma)}}, \tag{41}$$

where $x = -\log(1-z)$ and $C_n(\gamma)$ is a constant which must be calculated. Since we normalize $Ps_n(z;\gamma)$ by requiring that it equal the Legendre function $P_n(z)$ at the point $z = 0$, the constant $C_n(\gamma)$ can be determined by evaluating (41) and the Legendre polynomial of degree n at 0. We note that well-known formulas (such as those found on page 145 of [8]) make it easy to evaluate $P_n(0)$ in time independent of n. Once $C_n(\gamma)$ has been determined, the value of $Ps_n(z;\gamma)$ can be calculated at any z in the interval $[0, 1-\exp(-\beta))$ by first using the piecewise Chebyshev expansion

(39) to evaluate

$$\Psi S_n(x;\gamma) \quad \text{and} \quad \frac{d\Psi S_n}{dx}(x;\gamma) \tag{42}$$

and then plugging the resulting values into (41). When z is in $(-1-\exp(-\beta), 0)$, we use the well-known symmetry properties of $Ps_n(z;\gamma)$ (it is an even function when n is even and an odd function when n is odd) together with the procedure just described to evaluate it.

In the remainder of this section, we describe the method we use to solve ordinary differential equations, the technique used to construct the expansion (39) and an accelerated version of the algorithm obtained using the results of [21].

5.1. Adaptive solution of ordinary differential equations

The algorithm of this paper entails solving several ordinary differential equations. We use a fairly standard adaptive Chebyshev spectral solver to do so. We now briefly describe its operation in the case of the initial value problem

$$\begin{cases} \boldsymbol{y}'(t) = F(t, \boldsymbol{y}(t)), & a < t < b, \\ \boldsymbol{y}(a) = \boldsymbol{v} \end{cases} \tag{43}$$

where $F : \mathbb{R}^{n+1} \to \mathbb{R}^n$ is smooth and $\boldsymbol{v} \in \mathbb{R}^n$. The solver can be easily modified to apply to a terminal value problem.

The solver takes as input a positive integer k, an interval (a, b), a subroutine for evaluating the function F and the vector $\boldsymbol{v}$. It outputs n piecewise k^{th} order Chebyshev expansions, one for each of the components $y_i(t)$ of the solution $\boldsymbol{y}$ of (43).

The solver maintains two lists of subintervals of (a, b): one consisting of accepted intervals and the other of intervals which have yet to processed. Initially, the list of accepted intervals is empty and the list of intervals to process contains the single interval (a, b) It then operates as follows until the list of intervals to process is empty:

1. Find, in the list of interval to process, the interval (c, d) such that c is as small as possible and remove this interval from the list.

2. Solve the initial value problem

$$\begin{cases} \boldsymbol{u}'(t) = F(t, \boldsymbol{u}(t)), & c < t < d, \\ \boldsymbol{u}(c) = \boldsymbol{w} \end{cases} \tag{44}$$

   If $(c, d) = (a, b)$, then we take $\boldsymbol{w} = \boldsymbol{v}$. Otherwise, the value of the solution at the point c has already been approximated, and we use that estimate for $\boldsymbol{w}$ in (44).

   If the problem is linear, a straightforward Chebyshev spectral method (see, for instance, [24]) is used to solve (44). Otherwise, the trapezoidal method (see, for instance, [2]) is first used to produce an initial approximation y_0 of the solution and then Newton's method is applied to refine it. The linearized problems are solved using a straightforward Chebyshev spectral method.

   In any event, the result is a set of kth order Chebyshev expansions

$$u_i(x) \approx \sum_{j=0}^{k} \lambda_{ij}\, T_j\left(\frac{2}{d-c}x + \frac{c+d}{c-d}\right), \quad i = 1, \ldots, n, \tag{45}$$

   approximating the components $u_1, \ldots, u_n$ of the solution of (44).

3. Compute the quantities

$$\frac{\sqrt{\sum_{j=k/2}^{k} \lambda_{ij}^2}}{\sqrt{\sum_{j=0}^{k} \lambda_{ij}^2}}, \quad i = 1, \ldots, n, \tag{46}$$

where the λ_{ij} are the coefficients in the expansions (45). If any of the resulting values is larger than $100 \times \epsilon_0$, where ϵ_0 denotes machine zero for the IEEE double precision number scheme, then we split the interval into two halves $\left(c, \frac{c+d}{2}\right)$ and $\left(\frac{c+d}{2}, d\right)$ and place them on the list of intervals to process. Otherwise, we place the interval (c, d) on the list of accepted intervals.

At the conclusion of this procedure, we have k^{th} order Chebyshev expansions for each component of the solution, with the list of accepted intervals determining the partition for each expansion.

5.2. Construction of $\Psi S_n(x;\gamma)$

To construct $\Psi S_n(x;\gamma)$, we first calculate the values of the function $M_\nu(x;\gamma)$ and its first two derivatives with respect to x at 0. We do this by evaluating the logarithmic derivative

$$s(t) = \frac{f'(t)}{f(t)} \tag{47}$$

of the function

$$f(t) = S_n^{(3)}(it;\gamma)\sqrt{1+t^2} \tag{48}$$

and its derivative at the point 0. Since f is a solution of (22), s satisfies

$$s'(t) + (s(t))^2 + q_1(t) = 0, \tag{49}$$

where q_1 is the coefficient in (22) with χ taken to be equal to the Sturm-Liouville eigenvalue $\chi_n(\gamma)$. Moreover, from (20), it is apparent that

$$s(t) = -\gamma + \mathcal{O}\left(\frac{1}{t}\right). \tag{50}$$

Accordingly, we construct s by adaptively solving the terminal value problem

$$\begin{cases} s'(t) + (s(t))^2 + q_1(t) = 0, \quad 0 < t < c \\ s(c) = -\gamma, \end{cases} \tag{51}$$

where c is a suitable large constant (we take $c = 10^{30}$ in the experiments presented here). Because of Conjecture 2, we expect the function s to be well-behaved on the interval $(0, \infty)$ and for the cost of solving (51) to be slowly growing with γ and n.

Using the relations found in Section 2 and the definitions of Section 3, the values of $w(x) = M_\nu(1-\exp(-x);\gamma)(2-\exp(-x))$ and its first two derivatives at $x = 0$ can be expressed in terms of $s(0)$ and $s'(0)$. Indeed, w is the solution of the initial value problem

$$\begin{cases} w'''(x) + 4q_2(x)w'(x) + 2q_2'(x)w(x) = 0, \quad 0 \leqslant x < b, \\ w(0) = -\dfrac{1}{s(0)} \\ w'(0) = -\dfrac{1}{s(0)} \\ w''(0) = -\dfrac{1}{s(0)} + 2\dfrac{s'(0)}{s(0)}, \end{cases} \tag{52}$$

where q_2 is the coefficient in (21) with χ taken to be equal to $\chi_n(\gamma)$. The next step of our algorithm consists of solving (52) to construct a piecewise k^{th} order Chebyshev expansion for

$M_n(1-\exp(-x);\gamma)(2-\exp(-x))$. We let $0 = x_0 < x_1 < x_2 < \ldots < x_n = b$ be the partition on which this piecewise expansion is given.

Since

$$\begin{aligned} \Psi S_n(x;\gamma) &= \int_{\infty}^{x} \frac{\gamma}{M_n(1-\exp(-u);\gamma)(2-\exp(-u))}\, du \\ &\approx \int_{\beta}^{x} \frac{\gamma}{M_n(1-\exp(-u);\gamma)(2-\exp(-u))}\, du, \end{aligned} \tag{53}$$

spectral integration can be used to construct a kth order piecewise Chebyshev expansion for $\Psi S_n(x;\gamma)$. More explicitly, the final step of our algorithm consists of traversing the intervals (x_{i-1}, x_i) in decreasing order (i.e., $i = n, n-1, n \ldots, 1$) and, on each interval (x_{i-1}, x_i), constructing a kth order Chebyshev expansion representing $\Psi S_n(x;\gamma)$ by applying a $k \times k$ spectral integration matrix to the vector consisting of the coefficients in the Chebyshev expansion of $M_n(1-\exp(-x);\gamma)(2-\exp(-x))$ over the interval (x_{i-1}, x_i). The result is the piecewise Chebyshev expansion (39) for $\Psi S_n(x;\gamma)$.

The derivative of the phase function decays extremely slowly to 0 when the parameters γ and n are of small magnitude, and, in this event, it is necessary to choose β to be extremely close to 1 to achieve high accuracy in (53). This is what motivates the exponential change of variables used to obtain the form (21) of the reduced spheroidal wave equation and the decision to make β so large. We note that for most values of the parameters, β can be taken to be much smaller without losing accuracy.

We prefer to solve Appell's equation (14) over Kummer's equation (10) because of difficulties which are encountered when solving the latter numerically. The solution of Kummer's equation is the derivative of the phase function $\Psi S_n(x;\gamma)$. In cases in which (21) has a turning point, the derivative of $\Psi S_n(x;\gamma)$ decays rapidly to 0 once the turning point is reached. This creates numerical complications when solving Kummer's equation owing to the presence of the derivative of the phase function in the denominators of the some of the terms in (10). On the other hand, the modulus function which satisfies Appell's equation increasing on $(0, \beta)$ (indeed, it is absolutely monotone if our conjectures are correct).

5.3. Accelerated version of the algorithm

In [21], a numerical method for evaluating $\chi_n(\gamma)$ in time which is bounded independent of n and γ is described. It also allows for the $\mathcal{O}(1)$ calculation of the values of $\Psi S_n(z;\gamma)$ and its first few derivatives at the point $z = 0$. Using these quantities, the values of modulus function $M_n(1-\exp(-x);\gamma)(2-\exp(-x))$ and its first two derivatives at $x = 0$ can be easily obtained. The algorithm of this paper can be significantly accelerated by exploiting this capability. First, when the values of the modulus function $M_n(1-\exp(-x);\gamma)(2-\exp(-x))$ and its first two derivatives at $x = 0$ are known, there is no need to solve the terminal value problem (51). Second, when the value of $\Psi S_n(0;\gamma)$ is known, Formula (53) can be replaced with

$$\Psi S_n(x;\gamma) = \Psi S_n(0;\gamma) + \int_{0}^{x} \frac{\gamma}{M_n(1-\exp(-u);\gamma)(2-\exp(-u))}\, du. \tag{54}$$

Since we are no longer using (28) to determine the constant of integration, it is no longer necessary to calculate $\Psi S_n(x;\gamma)$ on a large interval. We instead construct a piecewise k^{th} Chebyshev expansion for it on the interval $[0, 30)$. This allows for the evaluation of $Ps_n(z;\gamma)$ for z in $[0, 1-\exp(-30))$, which more than suffices for most purposes.

6. Numerical Experiments

In this section, we present the results of numerical experiments which were conducted to illustrate the effectiveness of the algorithm of this article and to measure the dependence of the cost of representing $\Psi S_n(x;\gamma)$ on the parameters. As discussed in Section 3, for the purposes of numerical computation, the effective dimension of the space of functions with bandlimit γ is

$$\frac{2}{\pi}\gamma + \mathcal{O}\left(\log(\gamma)\right); \tag{55}$$

in particular, the number of prolate functions of interest depends on the bandlimit γ. Moreover, the qualitative behaviour of $Ps_n(z;\gamma)$ is best understood in terms of the ratio of n to γ. Accordingly, we introduce a new parameter σ which is related to n via

$$n = \text{round}\left(\gamma\sigma\right), \tag{56}$$

and the results presented here are discussed in terms of the parameters γ and σ rather than γ and n.

The code for our experiments was written in Fortran and compiled with version 11.1.0 of the GNU Fortran compiler. They were performed on a desktop computer equipped with an AMD Ryzen 3900x processor and 32GB of RAM. An implementation of our algorithm and code for conducting all of the experiments discussed here is available on GitHub at the following address:

`https://github.com/JamesCBremerJr/Prolates`

In some of these experiments, we compared the performance of our algorithm with that of the Osipov-Xiao-Rokhlin method [20]. Its running time is highly dependent on the dimension of the tridiagonal matrix formed in order to calculate the coefficients in the Legendre expansion of $Ps_n(z;\gamma)$. Most implementations use a highly conservative value for this dimension. The authors of [20], for instance, take it to be $1000 + n + \lfloor 1.1\gamma \rfloor$ in their implementation. In many cases, $Ps_n(z;\gamma)$ can be represented much more efficiently than this. The experiments of [22], though, suggest that the necessary dimension grows as $\mathcal{O}\left(n + \sqrt{n\gamma}\right)$. It is difficult, however, to find a simple formula which suffices in all cases of interest. Accordingly, our implementation of the Osipov-Rokhlin-Xiao algorithm initially takes the dimension to be

$$50 + \left\lfloor \frac{2}{\pi} n \right\rfloor + \lfloor \sqrt{\gamma n} \rfloor, \tag{57}$$

which we found to be sufficient for a large range of parameters, and then increases it adaptively as needed to ensure high accuracy. Our implementation can be found in the GitHub repository mentioned above.

6.1. The cost of representing $\Psi S_n(x;\gamma)$

In the experiments discussed here, we measured the cost to represent $\Psi S_n(x;\gamma)$ on the interval $[0, 30)$ using a piecewise k^{th} order Chebyshev expansion with $k = 29$. Table 1 and Figure 2 show the results.

Table 1 reports the number of coefficients required to represent the phase function on the interval $[0, 1-\exp(-30))$ for various ranges of values of γ and σ. For each row of the table, we first sampled 100 equispaced values of γ and 100 equispaced values of σ in the indicated ranges. Then, we constructed a piecewise Chebyshev expansion of $\Psi S_n(x;\gamma)$ for each of the $10,000$ pairs of sampled values and determined the number of coefficients in the largest expansion encountered.

Each plot on the left side of Figure 2 gives the number of Chebyshev coefficients in the expansion representing $\Psi S_n(x;\gamma)$ as function of γ for various values of σ, while each plot on the right side

Range of γ	Range of σ	Max Coefs	Range of γ	Range of σ	Max Coefs
100 to 500	$0.00 - 0.25$	420	10,000 to 50,000	$0.00 - 0.25$	540
	$0.25 - 0.50$	420		$0.25 - 0.50$	570
	$0.50 - 0.75$	360		$0.50 - 0.75$	570
	$0.75 - 1.00$	120		$0.75 - 1.00$	180
500 to 1,000	$0.00 - 0.25$	420	50,000 to 100,000	$0.00 - 0.25$	570
	$0.25 - 0.50$	450		$0.25 - 0.50$	570
	$0.50 - 0.75$	364		$0.50 - 0.75$	570
	$0.75 - 1.00$	130		$0.75 - 1.00$	180
1,000 to 5,000	$0.00 - 0.25$	450	100,000 to 500,000	$0.00 - 0.25$	630
	$0.25 - 0.50$	480		$0.25 - 0.50$	630
	$0.50 - 0.75$	450		$0.50 - 0.75$	630
	$0.75 - 1.00$	145		$0.75 - 1.00$	240
5,000 to 10,000	$0.00 - 0.25$	510	500,000 to 1,000,000	$0.00 - 0.25$	630
	$0.25 - 0.50$	510		$0.25 - 0.50$	660
	$0.50 - 0.75$	480		$0.50 - 0.75$	630
	$0.75 - 1.00$	150		$0.75 - 1.00$	300

Table 1: The cost of representing $\Psi S_n(x;\gamma)$ for various ranges of values of γ and σ. To generate the data presented in each row of this table, 100 equispaced values of γ and σ in the ranges indicated were sampled and a representation of $\Psi S_n(x;\gamma)$ over the interval $[0, 1-\exp(-30))$ was constructed for each of the $10,000$ resulting pairs of the parameters.

shows the number of Chebyshev coefficients in the expansion as a function of σ for various values of γ. A logarithmic scale is used for the x-axis in each plot on the left.

We immediately draw several conclusions from these experiments. First, we note that no more than 800 Chebyshev coefficients were required to represent any of the expansions formed during the course of these experiments. Second, we observe that while the cost to represent $\Psi S_n(x;\gamma)$ grows with γ, it does so at a modest rate. Indeed, the plots on the left side of Figure 2 indicate that for values of σ somewhat larger than $2/\pi$, the number of coefficients is essentially constant as a function of γ, while it increases sublogarithmically with γ for σ which are less than $2/\pi$. Finally, we observe from the plots on the right side of Figure 2 that a rapid drop in the cost of representing the phase function occurs when σ is close to $2/\pi$. For small values of σ, the reduced spheroidal wave equation has turning points on $(0,1)$ and its solutions are oscillatory only on part of that interval. However, starting when σ is a bit larger than $2/\pi$, the solutions of the reduced spheroidal wave equation are oscillatory on all of $(0,1)$. Evidently, the cost of representing $\Psi S_n(x;\gamma)$ in the oscillatory regime is bounded independent of γ, while the cost of representing it in the nonoscillatory regime grows sublogarithmically with γ.

6.2. The accuracy with which $Ps_n(z;\gamma)$ is evaluated

We now describe experiments conducted to measure the accuracy with which the algorithm of this paper evaluates the angular spheroidal wave functions of the first kind of order zero by comparison with the Osipov-Xiao-Rokhlin method. Table 2 and Figure 3 give the results.

Table 2 gives the accuracy of our algorithm for certain ranges of the parameters γ and σ. To generate the data presented in each row of this table, we first sampled 100 equispaced values of γ

Range of γ	Range of σ	Max Error	Range of γ	Range of σ	Max Error
100 to 500	$0.00 - 0.25$	6.74×10^{-14}	10,000 to 50,000	$0.00 - 0.25$	5.90×10^{-13}
	$0.25 - 0.50$	1.02×10^{-13}		$0.25 - 0.50$	9.07×10^{-13}
	$0.50 - 0.75$	3.91×10^{-13}		$0.50 - 0.75$	4.88×10^{-12}
	$0.75 - 1.00$	1.45×10^{-13}		$0.75 - 1.00$	2.10×10^{-12}
500 to 1,000	$0.00 - 0.25$	1.02×10^{-13}	50,000 to 100,000	$0.00 - 0.25$	8.62×10^{-13}
	$0.25 - 0.50$	1.49×10^{-13}		$0.25 - 0.50$	1.42×10^{-12}
	$0.50 - 0.75$	7.02×10^{-13}		$0.50 - 0.75$	2.12×10^{-11}
	$0.75 - 1.00$	2.09×10^{-13}		$0.75 - 1.00$	2.03×10^{-11}
1,000 to 5,000	$0.00 - 0.25$	2.09×10^{-13}	100,000 to 500,000	$0.00 - 0.25$	1.94×10^{-12}
	$0.25 - 0.50$	3.25×10^{-13}		$0.25 - 0.50$	3.39×10^{-12}
	$0.50 - 0.75$	2.14×10^{-12}		$0.50 - 0.75$	5.32×10^{-11}
	$0.75 - 1.00$	5.54×10^{-13}		$0.75 - 1.00$	5.44×10^{-11}
5,000 to 10,000	$0.00 - 0.25$	2.76×10^{-13}	500,000 to 1,000,000	$0.00 - 0.25$	2.87×10^{-12}
	$0.25 - 0.50$	4.31×10^{-13}		$0.25 - 0.50$	4.51×10^{-12}
	$0.50 - 0.75$	3.13×10^{-12}		$0.50 - 0.75$	1.09×10^{-10}
	$0.75 - 1.00$	1.10×10^{-12}		$0.75 - 1.00$	7.52×10^{-11}

Table 2: The accuracy with which $Ps_n(z;\gamma)$ is evaluated for various ranges of values of γ and σ.

and σ in the ranges indicated. Then, for each of the $10,000$ pairs of sampled values, we evaluated $Ps_n(z;\gamma)$ at 100 equispaced points $\{x_k\}$ in the interval $(0,1)$ using the algorithm of this paper and the Osipov-Xiao-Rokhlin method. The largest absolute error observed is reported in Table 2.

Figure 3 contains plots showing the dependence of the accuracy of our algorithm on γ and σ. For each pair of parameters considered, $Ps_n(z;\gamma)$ was evaluated at 100 equispaced points $\{x_k\}$ on the interval $(0,1)$ and the largest absolute error was determined. Each plot on the left side of that figure gives the accuracy with which $Ps_n(z;\gamma)$ is evaluated as function of γ for various values of σ, while each plot on the right side plots the accuracy as a function of σ for various values of γ. A logarithmic scale is used for the x-axis in each plot on the left.

As expected, accuracy is lost as both γ and σ increase. This occurs because the magnitude of $\Psi S_n(x;\gamma)$ increases with both of these variables and the accuracy with which the sine function is evaluated decreases with the magnitude of its argument. We note that the condition number of the reduced spheroidal wave equation and the condition number of evaluation of its solutions increases with the parameters γ and σ as well, so some loss of precision is expected. We also observe that the largest error observed during the course of these experiments was approximately 10^{-10}, and this was only for values of γ near $1,000,000$.

6.3. The time required to construct $\Psi S_n(x;\gamma)$

In these experiments, we measured the time required to calculate the phase function $\Psi S_n(x;\gamma)$ using both the accelerated and unaccelerated algorithm described in this paper. In some of these experiments, we compared it with the time taken by the Osipov-Xiao-Rokhlin method to construct the Legendre expansion representing $Ps_n(z;\gamma)$. Table 3 and Figures 4 and 5 give the results.

Range of γ	Range of σ	Average Time Unaccelerated	Average time Accelerated	Average time Rokhlin, et. al.	Ratio
100 to 500	$0.00 - 0.25$	5.35×10^{-03}	3.05×10^{-04}	9.76×10^{-05}	0.32
	$0.25 - 0.50$	3.32×10^{-03}	2.62×10^{-04}	1.31×10^{-04}	0.50
	$0.50 - 0.75$	1.90×10^{-03}	1.16×10^{-04}	1.71×10^{-04}	1.47
	$0.75 - 1.00$	1.85×10^{-03}	6.95×10^{-05}	2.11×10^{-04}	3.04
500 to 1,000	$0.00 - 0.25$	6.78×10^{-03}	3.54×10^{-04}	1.85×10^{-04}	0.52
	$0.25 - 0.50$	5.42×10^{-03}	3.43×10^{-04}	2.87×10^{-04}	0.84
	$0.50 - 0.75$	2.24×10^{-03}	1.53×10^{-04}	3.96×10^{-04}	2.58
	$0.75 - 1.00$	1.97×10^{-03}	9.26×10^{-05}	4.90×10^{-04}	5.29
1,000 to 5,000	$0.00 - 0.25$	7.20×10^{-03}	4.04×10^{-04}	5.73×10^{-04}	1.42
	$0.25 - 0.50$	6.94×10^{-03}	4.18×10^{-04}	1.09×10^{-03}	2.61
	$0.50 - 0.75$	3.26×10^{-03}	2.11×10^{-04}	1.48×10^{-03}	7.01
	$0.75 - 1.00$	2.16×10^{-03}	9.84×10^{-05}	1.87×10^{-03}	19.08
5,000 to 10,000	$0.00 - 0.25$	7.40×10^{-03}	4.36×10^{-04}	1.34×10^{-03}	3.08
	$0.25 - 0.50$	7.27×10^{-03}	4.54×10^{-04}	2.67×10^{-03}	5.88
	$0.50 - 0.75$	4.09×10^{-03}	2.47×10^{-04}	3.65×10^{-03}	14.80
	$0.75 - 1.00$	2.47×10^{-03}	9.88×10^{-05}	4.63×10^{-03}	46.87
10,000 to 50,000	$0.00 - 0.25$	7.58×10^{-03}	4.74×10^{-04}	5.12×10^{-03}	10.79
	$0.25 - 0.50$	7.53×10^{-03}	4.99×10^{-04}	1.04×10^{-02}	20.96
	$0.50 - 0.75$	4.94×10^{-03}	2.94×10^{-04}	1.45×10^{-02}	49.39
	$0.75 - 1.00$	3.12×10^{-03}	1.02×10^{-04}	1.81×10^{-02}	177.52
50,000 to 100,000	$0.00 - 0.25$	7.71×10^{-03}	5.04×10^{-04}	1.24×10^{-02}	24.75
	$0.25 - 0.50$	7.78×10^{-03}	5.33×10^{-04}	2.58×10^{-02}	48.36
	$0.50 - 0.75$	5.49×10^{-03}	3.32×10^{-04}	3.63×10^{-02}	109.16
	$0.75 - 1.00$	3.84×10^{-03}	1.28×10^{-04}	4.91×10^{-02}	381.27
100,000 to 500,000	$0.00 - 0.25$	7.07×10^{-03}	5.73×10^{-04}	5.40×10^{-02}	94.38
	$0.25 - 0.50$	1.27×10^{-02}	1.14×10^{-03}	3.14×10^{-01}	275.27
	$0.50 - 0.75$	1.21×10^{-02}	9.41×10^{-04}	5.47×10^{-01}	582.02
	$0.75 - 1.00$	9.30×10^{-03}	4.18×10^{-04}	7.39×10^{-01}	1766.48
500,000 to 1,000,000	$0.00 - 0.25$	1.06×10^{-02}	9.22×10^{-04}	2.96×10^{-01}	321.57
	$0.25 - 0.50$	1.86×10^{-02}	1.72×10^{-03}	$1.07 \times 10^{+00}$	619.20
	$0.50 - 0.75$	1.54×10^{-02}	1.19×10^{-03}	$1.56 \times 10^{+00}$	1306.14
	$0.75 - 1.00$	1.20×10^{-02}	4.99×10^{-04}	$1.98 \times 10^{+00}$	3979.82

Table 3: The average time (in seconds) required by the accelerated and unaccelerated versions of the algorithm of this paper to construct the phase function $\Psi S_n(x;\gamma)$ they use to represent $Ps_n(z;\gamma)$, as well as the time required by the Osipov-Xiao-Rokhlin method to construct the Legendre expansion it uses to represent $Ps_n(z;\gamma)$. The "Ratio" column reports the ratio of the time taken by the Osipov-Xiao-Rokhlin method to the time taken by the accelerated version of the algorithm of this paper.

Table 3 gives the average time required to construct the phase function $\Psi S_n(x;\gamma)$ using the accelerated and unaccelerated versions of this algorithm as well as the average time taken by the

Osipov-Xiao-Rokhlin algorithm to construct the Legendre expansion representing $Ps_n(z;\gamma)$ for various ranges of the parameters γ and σ. To generate the data for each row of the table, first 100 equispaced values of the each of the parameters γ and σ were sampled. Then, for each of the $10,000$ pairs of sampled values of the parameter, the phase function $\Psi S_n(x;\gamma)$ representing $Ps_n(z;\gamma)$ was constructed using both the accelerated and unaccelerated algorithms of this paper and a Legendre expansion representing $Ps_n(z;\gamma)$ was constructed with the Osipov-Xiao-Rokhlin method. The average time taken by each of these procedures is reported. The column labelled 'Ratio' in Table 3 gives the ratio of the average time taken by the Osipov-Xiao-Rokhlin method to the average time taken by the accelerated version of our algorithm.

Each of the plots on the left side of Figure 4 gives the time required by the accelerated version of our algorithm to construct $\Psi S_n(x;\gamma)$ as a function of γ for several different values of σ. Similarly, each plot on the right side of Figure 4 gives the time needed to construct $\Psi S_n(x;\gamma)$ as a function of σ for various values of γ.

Figure 5 contains plots comparing the time required to construct $\Psi S_n(x;\gamma)$ using the accelerated version of the method of this paper with the time required by the Osipov-Xiao-Rokhlin algorithm to construct the Legendre expansion representing $Ps_n(z;\gamma)$. Each plot on the left side of Figure 5 gives these quantities as functions of γ for a fixed σ, while the plots on the right side of the figure gives these quantities as functions of σ for a fixed γ. We choose the range of γ displayed in each plot on the right in order to emphasize the break-even point between the two methods.

From these experiments, we conclude that the time required to construct $\Psi S_n(x;\gamma)$ grows sublogarithmically with γ and is bounded independent of σ. Moreover, we see that the Osipov-Xiao-Rokhlin algorithm is faster for small values of the parameter, but for $\gamma\sigma > 250$ or so, the accelerated version of the algorithm of this paper becomes more efficient, and it is much more efficient at large values of γ.

6.4. The time required to evaluate $Ps_n(z;\gamma)$

In this final set of experiments, we measured the time required to evaluate $Ps_n(z;\gamma)$ using the phase function $\Psi S_n(x;\gamma)$ and compared it to the time needed to evaluate the Legendre expansion used by the Osipov-Xiao-Rokhlin to represent $Ps_n(z;\gamma)$. Table 4 and Figures 6 give the results.

Table 4 gives the average time required to evaluate $Ps_n(z;\gamma)$ using the the phase function $\Psi S_n(x;\gamma)$ as well as the average time required to evaluate the Legendre expansion used by the Osipov-Xiao-Rokhlin algorithm to represent $Ps_n(z;\gamma)$ for various ranges of the parameters γ and σ. To generate the data for each row of the table, we first sampled 20 equispaced values of the each of the parameters γ and σ. Then, for each of the 400 pairs of sampled values of the parameter, the phase function $\Psi S_n(x;\gamma)$ representing $Ps_n(z;\gamma)$ was constructed using the algorithm of this paper and a Legendre expansion representing $Ps_n(z;\gamma)$ was constructed with the Osipov-Xiao-Rokhlin method. Next, for each pair of the parameters γ and n, $Ps_n(z;\gamma)$ was evaluated at 100 equispaced points on the interval $(0,1)$. The average time taken to perform these $40,000$ evaluations is reported.

Each of the plots on the left side of Figure 6 gives the time required to evaluate $\Psi S_n(x;\gamma)$ as a function of γ for several different values of σ. Similarly, each plot on the right side of Figure 4 gives the time needed to evaluate $Ps_n(z;\gamma)$ as a function of σ for various values of γ.

We omit the analog of Figure 5 comparing the time required to evaluate the phase function $\Psi S_n(x;\gamma)$ used by the algorithm of this paper to represent $Ps_n(z;\gamma)$ and the time required to evaluate it using the Legendre expansion used by Xiao-Osipov-Rokhlin method to represent $Ps_n(z;\gamma)$. This is because, even for small values of γ and σ, the phase function method is considerably faster.

We conclude from these experiments that the time required to evaluate $Ps_n(z;\gamma)$ using the phase function $\Psi S_n(x;\gamma)$ is largely independent of the parameters γ and σ.

Range of γ	Range of σ	Average time Phase	Average time Rokhlin, et. al.	Ratio
100 to 500	$0.00 - 0.25$	1.22×10^{-07}	1.66×10^{-06}	13.67
	$0.25 - 0.50$	1.14×10^{-07}	2.17×10^{-06}	18.99
	$0.50 - 0.75$	1.36×10^{-07}	2.44×10^{-06}	17.88
	$0.75 - 1.00$	1.16×10^{-07}	2.70×10^{-06}	23.30
500 to 1,000	$0.00 - 0.25$	1.36×10^{-07}	3.28×10^{-06}	24.08
	$0.25 - 0.50$	1.18×10^{-07}	4.59×10^{-06}	38.74
	$0.50 - 0.75$	1.17×10^{-07}	5.29×10^{-06}	45.25
	$0.75 - 1.00$	1.18×10^{-07}	5.89×10^{-06}	49.92
1,000 to 5,000	$0.00 - 0.25$	1.55×10^{-07}	9.89×10^{-06}	63.71
	$0.25 - 0.50$	1.26×10^{-07}	1.57×10^{-05}	124.06
	$0.50 - 0.75$	1.17×10^{-07}	1.86×10^{-05}	158.33
	$0.75 - 1.00$	1.17×10^{-07}	2.10×10^{-05}	178.54
5,000 to 10,000	$0.00 - 0.25$	1.62×10^{-07}	2.23×10^{-05}	137.12
	$0.25 - 0.50$	1.30×10^{-07}	3.73×10^{-05}	287.03
	$0.50 - 0.75$	1.18×10^{-07}	4.49×10^{-05}	378.10
	$0.75 - 1.00$	1.18×10^{-07}	5.09×10^{-05}	429.64
10,000 to 50,000	$0.00 - 0.25$	1.66×10^{-07}	8.18×10^{-05}	491.98
	$0.25 - 0.50$	1.32×10^{-07}	1.43×10^{-04}	1088.13
	$0.50 - 0.75$	1.19×10^{-07}	1.74×10^{-04}	1465.68
	$0.75 - 1.00$	1.17×10^{-07}	1.98×10^{-04}	1683.48
50,000 to 100,000	$0.00 - 0.25$	1.66×10^{-07}	1.99×10^{-04}	1196.92
	$0.25 - 0.50$	1.35×10^{-07}	3.58×10^{-04}	2645.23
	$0.50 - 0.75$	1.21×10^{-07}	4.35×10^{-04}	3597.88
	$0.75 - 1.00$	1.20×10^{-07}	4.96×10^{-04}	4129.21
100,000 to 500,000	$0.00 - 0.25$	1.61×10^{-07}	7.87×10^{-04}	4864.34
	$0.25 - 0.50$	1.39×10^{-07}	1.61×10^{-03}	11542.75
	$0.50 - 0.75$	1.33×10^{-07}	2.75×10^{-03}	20682.52
	$0.75 - 1.00$	1.35×10^{-07}	3.27×10^{-03}	24266.13
500,000 to 1,000,000	$0.00 - 0.25$	1.70×10^{-07}	2.49×10^{-03}	14689.04
	$0.25 - 0.50$	1.78×10^{-07}	1.28×10^{-02}	72054.88
	$0.50 - 0.75$	1.64×10^{-07}	1.73×10^{-02}	105582.86
	$0.75 - 1.00$	1.58×10^{-07}	1.80×10^{-02}	114213.05

Table 4: The average time (in seconds) required by the algorithm of this paper and by the Osipov-Xiao-Rokhlin method to evaluate $Ps_n(z;\gamma)$. The "Ratio" column reports the ratio of the time taken by the two methods.

7. Conclusions

It is well known that many second order differential equations have solutions whose logarithms are easier to represent than the solutions themselves. Historically, this observation has mainly been used to construct asymptotic expansions of the solutions of such equations. Here we suggest a more direct approach: the numerical computation of the logarithms. We discuss the results of experiments which indicate such an approach leads to a method for the numerical evaluation of the prolate spheroidal wave functions of order zero whose running time grows much more slowly with bandlimit and characteristic exponent than standard algorithms. Moreveor, the algorithm presented here can be viewed as a template suitable for application to many other families of special functions satisfying second order differential equations, such as the Jacobi polynomials and Hermite functions.

We rely on experimental evidence for our claims. It would be of great interest to prove a bound on the cost of representing the phase function $\Psi S_n(x;\gamma)$ or a related function using piecewise polynomial expansions. Proving the conjectures made in this article regarding the associated modulus function might provide a good starting point for such an endeavor. Formulas which imply the monotonicity properties of many related second order differential equations (such as those established in [6] and [7]) have been proved using Koornwinder's addition formula for Jacobi functions [13]. An analagous result for the spheroidal wave functions would most likely lead to proofs of the conjectures made in Section 4.

We believe it is possible to eliminate the dependence of the running time of the algorithm described here on the bandlimit γ. The cost of representing the logarithms of the WKB solution in regions bounded away from the turning points of the reduced spheroidal wave equation appears to be independent of γ. It is only near the turning point where the complexity increases with γ. A more sophisticated approach, which used an alternate representation of $Ps_n(z;\gamma)$ near turning points, would most likely yield an $\mathcal{O}(1)$ algorithm for evaluation the prolate spheroidal wave functions of order zero.

Finally, we note that the methodology discussed here and in [21] can be applied to the spheroidal wave functions of nonzero orders. We believe the conjectures of Section 4 extend essentially without modification to that equation. The only additional difficulty is that the expansions used in [21] to evaluate the Sturm-Liouville eigenvalues of the spheroidal wave functions would depend on three variables instead of two, and be correspondingly larger and cost more to evaluate.

8. Acknowledgements

The author was supported in part by NSERC Discovery grant RGPIN-2021-02613, and by NSF grants DMS-1818820 and DMS-2012487.

References

[1] Appell, P. Sur la transformation des équations différentielles linéaires. *Comptes Rendus 91* (1880), 211–214.

[2] Ascher, U. M., and Petzold, L. R. *Computer Methods for Ordinary Differential Equations and Differential-Algebraic Equations.* Society for Industrial and Applied Mathematics, USA, 1998.

[3] Bogaert, I., Michiels, B., and Fostier, J. $O(1)$ computation of Legendre polynomials and Gauss-Legendre nodes and weights for parallel computing. *SIAM Journal on Scientific Computing 34* (2012), C83–C101.

[4] *NIST Digital Library of Mathematical Functions.* http://dlmf.nist.gov/, Release 1.1.0 of 2020-12-15. F. W. J. Olver, A. B. Olde Daalhuis, D. W. Lozier, B. I. Schneider, R. F. Boisvert, C. W. Clark, B. R. Miller, B. V. Saunders, H. S. Cohl, and M. A. McClain, eds.

[5] Dunster, T. Uniform asymptotic expansions for prolate spheroidal functions with large parameters. *SIAM Journal on Mathematical Analysis 17*, 6 (1986), 1495–1524.

[6] Durand, L. Nicholson-type integrals for products of Gegenbauer functions and related topics. In *Theory and Application of Special Functions*, R. A. Askey, Ed. Academic Press, 1975, pp. 353–374.

[7] Durand, L. Product formulas and Nicholson-type integrals for Jacobi functions. I: Summary of results. *Siam Journal on Mathematical Analysis 9* (1978), 76–86.

[8] Erdélyi, A., et al. *Higher Transcendental Functions*, vol. I. McGraw-Hill, 1953.

[9] Gil, A., Segura, J., and Temme, N. *Numerical methods for special functions.* SIAM, 2007.

[10] Hartman, P. On differential equations and the function $J_\mu^2 + Y_\mu^2$. *American Journal of Mathemtics 83* (1961), 154–188.

[11] Hartman, P. On differential equations, Volterra equations and the function $J_\mu^2 + Y_\mu^2$. *American Journal of Mathemtics 95* (1973), 553–593.

[12] Hille, E. *Ordinary Differential Equations in the Complex Plane.* John Wiley and Sons, 1976.

[13] Koornwinder, T. The addition formula for Jacobi polynomials I: summary of results. *Indagationes Mathematicae (Proceedings) 75*, 2 (1972), 188–191.

[14] Kummer, E. De generali quadam aequatione differentiali tertti ordinis. *Progr. Evang. Köngil. Stadtgymnasium Liegnitz* (1834).

[15] Landau, H. J., and Widom, H. Eigenvalue distribution of time and frequency limiting. *Journal of Mathematical Analysis and Applications 77* (1980), 469–481.

[16] Meixner, J., and Schäfke, F. *Mathieusche Funktionen und Sphäroidfunktionen.* Springer-Verlag, 1954 (in German).

[17] Miller, P. D. *Applied Asymptotic Analysis.* American Mathematical Society, 2006.

[18] Olver, F. W. *Asymptotics and Special Functions.* A.K. Peters, 1997.

[19] Osipov, A., and Rokhlin, V. On the evaluation of prolate spheroidal wave functions and associated quadrature rules. *Applied and Computational Harmonic Analysis 36*, 1 (2014), 108–142.

[20] Osipov, A., Rokhlin, V., and Xiao, H. *Prolate Spheroidal Wave Functions of Order* 0. Springer, 2013.

[21] Rehan, R., and Bremer, J. An $\mathcal{O}(1)$ algorithm for the numerical evaluation of the Sturm-Liouville eigenvalues of the spheroidal wave functions of order zero.

[22] Schmutzhard, S., Hrycak, T., and Feichtinger, H. A numerical study of the Legendre-Galerkin method for the evaluation of the prolate spheroidal wave functions. *Numerical Algorithms 68* (2015), 1017–1398.

[23] Slepian, D., and Pollak, H. Prolate spheroidal wave functions, Fourier analysis and uncertainty — I. *The Bell System Technical Journal 40* (1961), 43–64.

[24] Trefethen, N. *Approximation Theory and Approximation Practice.* Society for Industrial and Applied Mathematics, Philadelphia, PA, 2013.

[25] Widder, D. *The Laplace Transform.* Princeton University Press, 1946.

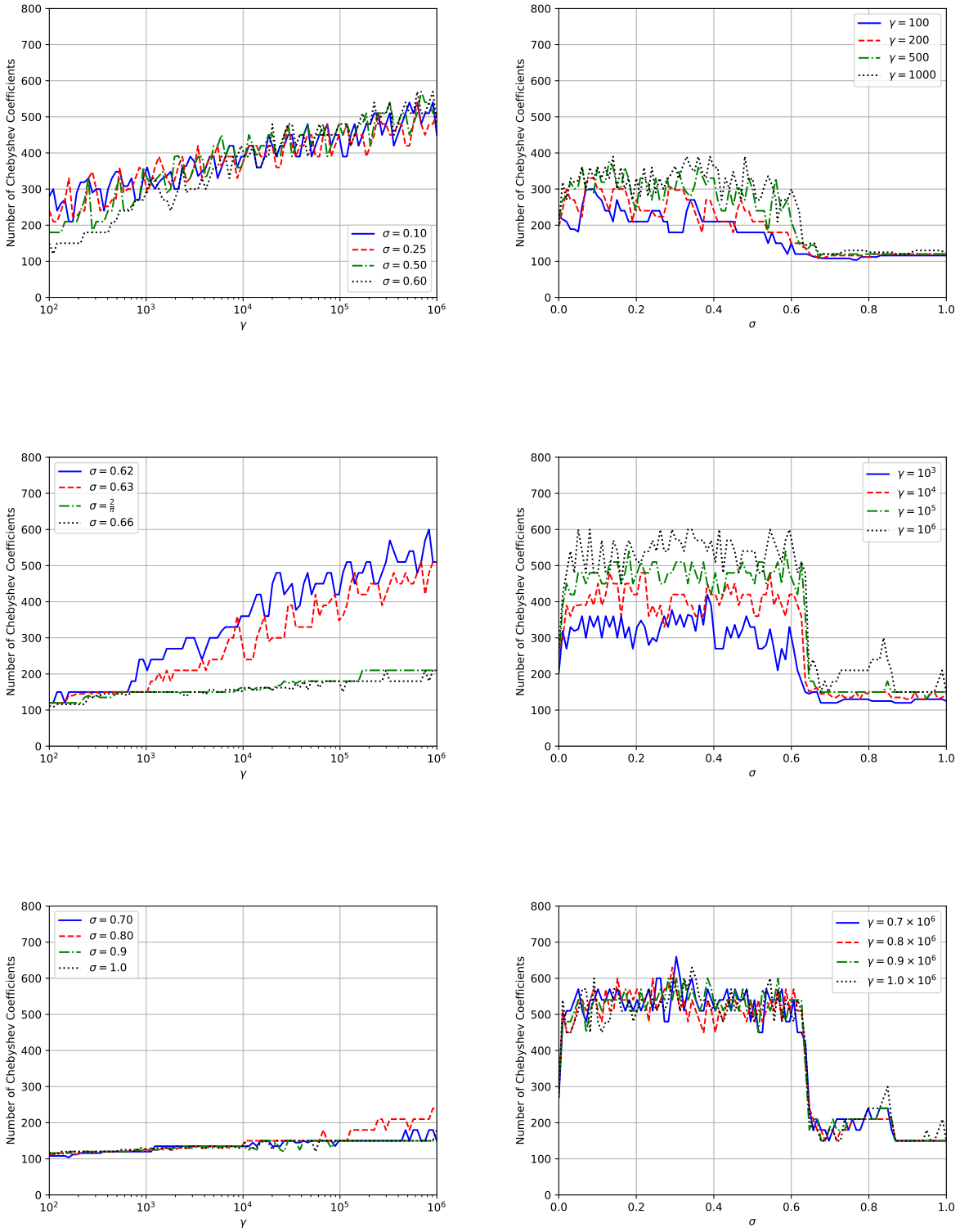

Figure 2: The number of Chebyshev coefficients required to represent $\Psi S_n(\gamma)$. Each of the graphs on the left gives the number of coefficients as function of γ for several values of σ, while the plots on the right give the number of coefficients as a function of σ for several values of γ. A logarithmic scale is used for the x-axis in each of the plots on the left.

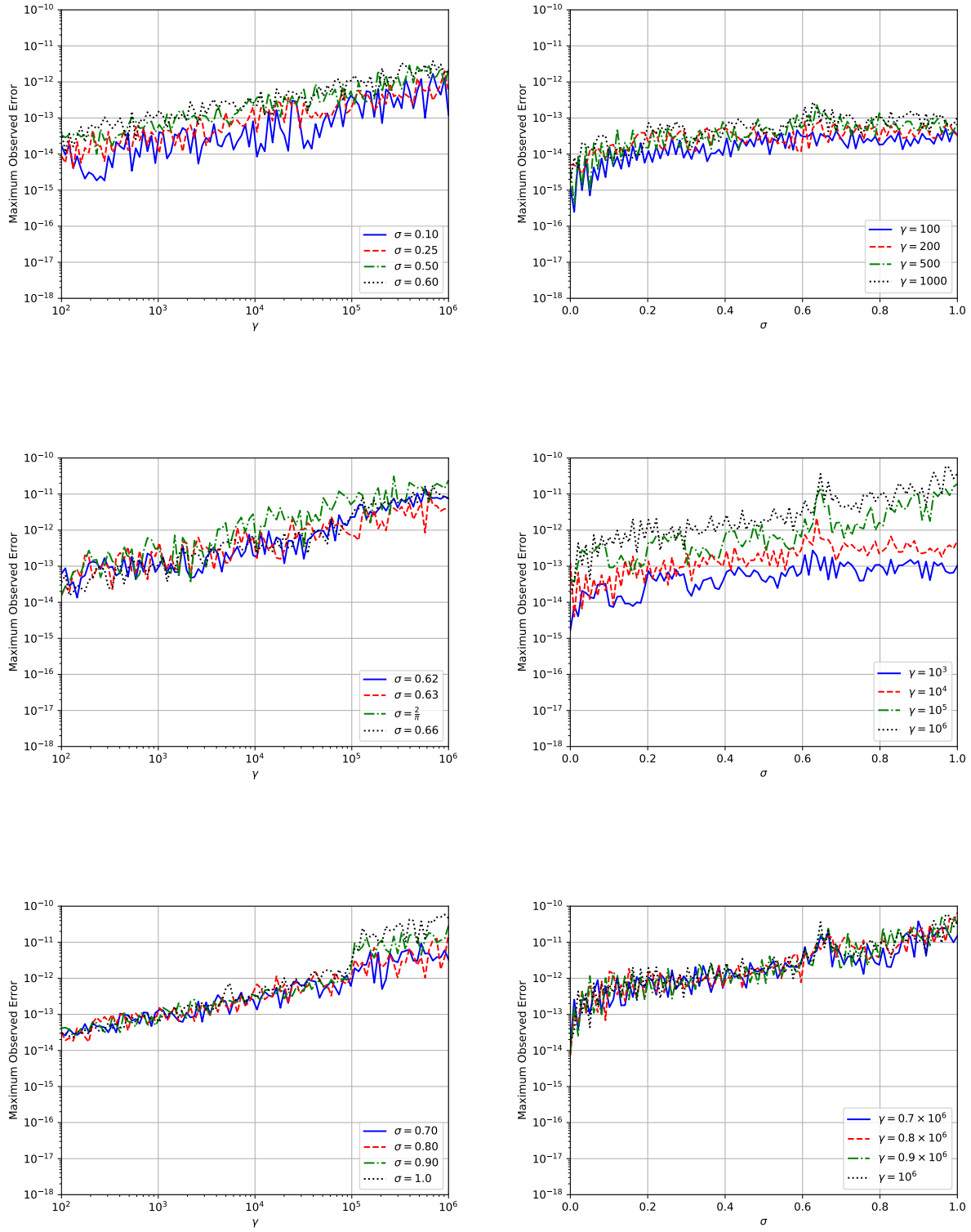

Figure 3: The accuracy with which $Ps_n(\gamma)$ is evaluated. Each of the graphs on the left gives the maximum observed error as a function of γ for several values of σ, while the plots on the right give the maximum observed error as a function of σ for several values of γ. A logarithmic scale is used for the x-axis in each of the plots on the left.

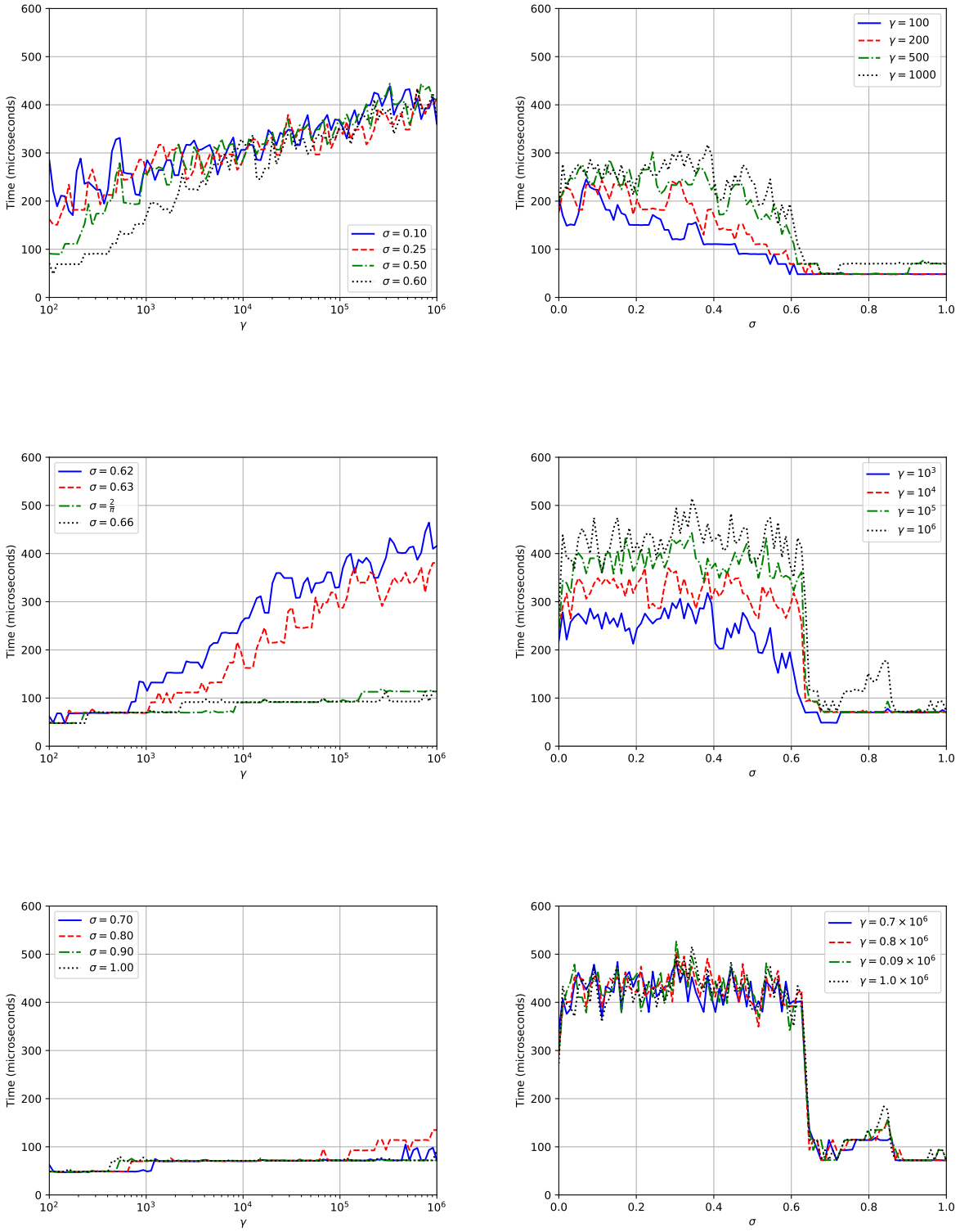

Figure 4: The time (in microseconds) required by the accelerated version of the algorithm of this paper to construct $\Psi S_n(\gamma; z)$. Each of the graphs on the left gives the time required as a function of γ for several values of σ, while the plots on the right give the required time as a function of σ for several values of γ. A logarithmic scale is used for the x-axis in each of the plots on the left.

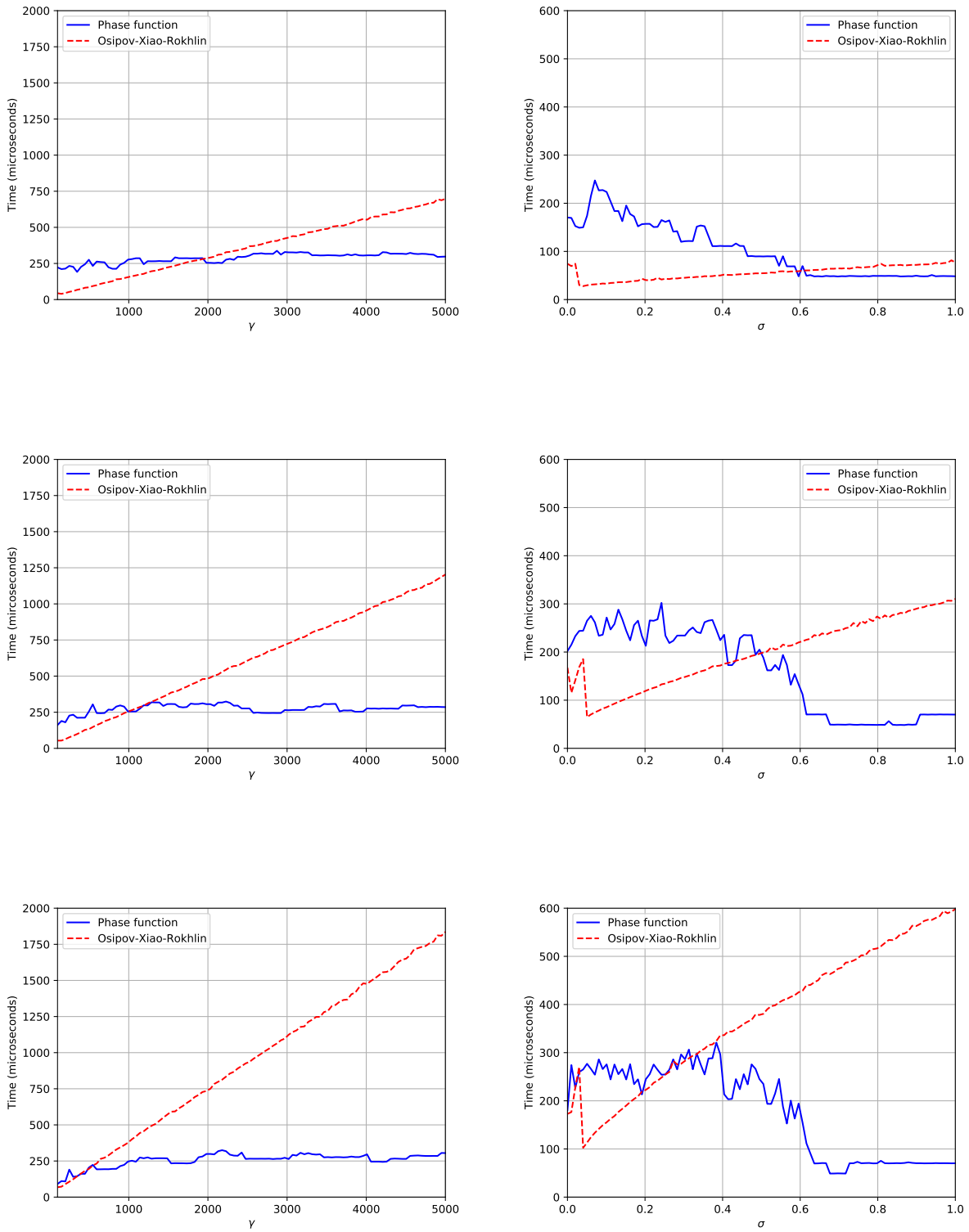

Figure 5: A comparison of the time required to construct a representation of $Ps_n(z;\gamma)$ using the accelerated version of the algorithm of this paper and the Xiao-Osipov-Rokhlin method. Each plot on the left gives these quanitites as a function of gamma for a fixed value of σ. From top to bottom, $\sigma = 0.10$, $\sigma = 0.25$ and $\sigma = 0.50$. Each plot on the right gives these quanitites as a function of sigma for fixed values of γ. From top to bottom, $\gamma = 100$, $\gamma = 500$ and $\gamma = 1,000$.

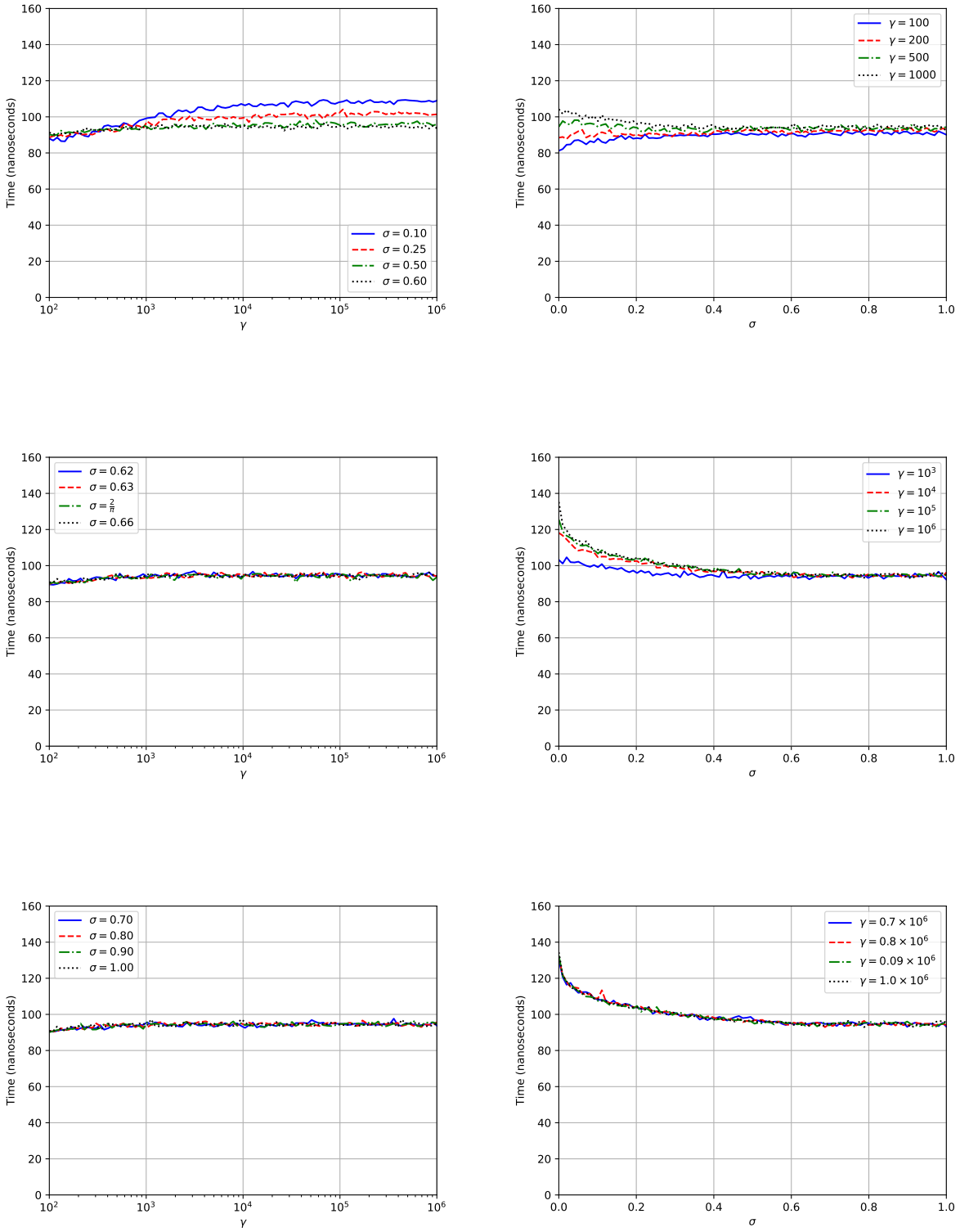

Figure 6: The time (in nanoseconds) required to evaluate $Ps_n(z;\gamma)$ using the algorithm of this paper. Each of the graphs on the left gives the time required as a function of γ for several values of σ, while the plots on the right give the required time as a function of σ for several values of γ. A logarithmic scale is used for the x-axis in each of the plots on the left.